

ABSTRACT

INELASTIC PROTON SCATTERING

FROM ^{48}Ca

By

Carl Jerome Maggiore

Inelastic proton scattering from the nucleus ^{48}Ca has been performed at four energies: 25.11, 29.83, 35.00, and 40.21 MeV, using the proton beam from the MSU sector-focused cyclotron. Cross sections were taken every five degrees from 13° to 100° with Ge(Li) counters fabricated at this laboratory. The overall resolution obtained was less than 30 keV at all energies.

The elastic scattering from ^{48}Ca was compared with the elastic scattering from ^{40}Ca using the optical model. It was found that the relative matter distributions are in agreement with the predictions of the $A^{1/3}$ law.

The inelastic scattering revealed several previously unreported excited states in ^{48}Ca . Angular momentum transfers for most of the states were obtained by comparison of the shapes of the angular distributions to those of known L. Where possible, spin assignments are inferred on the basis of this and other data.

The experimental angular distributions are compared with calculated distributions using the collective model distorted wave Born approximation. The nuclear deformations obtained are used to calculate the vibrational model parameters and the reduced transition probabilities. The results are compared with previous inelastic alpha scattering experiments and inelastic electron scattering

results. The energy dependence of the results and the sensitivity of the deformations to the optical model parameters were studied.

INELASTIC PROTON SCATTERING

FROM ^{48}Ca

By

Carl Jerome Maggiore

A THESIS

Submitted to
Michigan State University
in partial fulfillment of the requirements
for the degree of

DOCTOR OF PHILOSOPHY

Department of Physics

1971

For Jan

ACKNOWLEDGEMENTS

I would like to give special thanks to Charles Gruhn, my advisor, for his patient and unlimited willingness to help throughout the last four years. I am unable to adequately express the debt of gratitude that I owe him.

Special thanks are also due to Barry Preedom for help with the calculations, the data taking, and being there when needed. To Thomas Kuo who worked closely with me throughout the experiment many thanks are due. Without him the work could not have been done.

And for help and understanding in the non-technical aspects of this work my deepest thanks to my parents and my wife, Jan.

TABLE OF CONTENTS

Acknowledgments	iii
List of Tables	vi
List of Figures	vii
1. Introduction	i
2. Experimental Procedures	iii
2.1 Modifications to the Goniometer	iii
2.2 Target Storage System	iv
2.3 Cyclotron and Beam Transport	vi
2.4 Detectors	ix
2.5 Electronics	x
2.6 Data Acquisition	xi
3. Data Analysis	xviii
3.1 Angle Calibration	xviii
3.2 Normalization	xix
3.3 Excitation Energies	xxii
3.4 Cross Sections	xxv
4. Optical Model Studies	xxvi
4.1 Optical Model for DWBA Calculations	xxvi
4.2 Optical Model Difference between ^{40}Ca and ^{48}Ca	xxxi
5. Theoretical Analysis	xlvi
5.1 DWBA Theory	xlvi
5.2 Collective Model	xlix

5.3	Vibrational Model	1
5.4	Calculations	liii
6.	Results	lx
6.1	States below 5 MeV	lx
6.2	States between 5 and 6 MeV	lxvi
6.3	States between 6 and 7 MEV	lxxiii
6.4	States between 7 and 8 MeV	lxxiii
6.5	States between 8 and 9 MeV	lxxiv
6.6	Summary	lxxviii
6.7	Comparison with Theory	lxxxii
	Bibliography	lxxxiv
	Appendices	
I.	Detector Fabrication and Testing	lxxxvii
I.1	Choice of Ge(Li)	lxxxvii
I.2	Fabrication	lxxxviii
I.3	Packaging	xcii
I.4	Testing	xcv
I.5	Radiation Damage	xcvii
I.6	Other Ge(Li) Detectors	ciii
II.	Experimental Data	cviii
II.1	Theoretical Angular Distributions	cviii
II.2	Plotted Angular Distributions	cxiii
II.3	Tabulated Angular Distributions	cxliv
II.4	Tabulated Nuclear Deformations	clxxvi
II.5	Quantities Calculated from the Nuclear Deformations	clxxxii

LIST OF TABLES

2.1	Contributions to the energy resolution	xiii
3.1	Isotopic analysis of the target	xxi
3.2	Contributions to the uncertainty in absolute normalization	xxi
3.3	Excitation energies of ^{48}Ca	xxiv
4.1	Fricke's average optical parameters	xxvii
4.2	Potential well depths using Fricke geometry	xxviii
4.3	Potential well depths with equal real and imaginary geometries	xxviii
4.4	Differences in the optical model parameters for ^{48}Ca and ^{40}Ca	xxxviii
6.1	Upper limits on the $0+$ cross sections	lxvii
6.2	Comparison of the nuclear deformations	lxxxii
I.1	Contributions to the energy resolution	c

LIST OF FIGURES

2.1	Cyclotron and beam layout	vii
2.2	Ge(Li) electronics	xii
2.3	Typical 25 MeV spectrum	xiv
2.4	Typical 30 MeV spectrum	xv
2.5	Typical 35 MeV spectrum	xvi
2.6	Typical 40 MeV spectrum	xvii
4.1	Optical model fit with R = I geometry	xxix
4.2	Optical model fit with Fricke geometry	xxx
4.3	40 MeV χ^2 surface	xxxiv
4.4	35 MeV χ^2 surface	xxxx
4.5	30 MeV χ^2 surface	xxxvi
4.6	25 MeV χ^2 surface	xxxvii
4.7	Ratio of elastic angular distributions	xl
4.8	Optical model radii with $U_{\text{sym}} = 0$	xli
4.9	Optical model radii with $U_{\text{sym}} = 4.4$ MeV	xlii
4.10	Optical model radii with $U_{\text{sym}} = 0$ and unequal geometries	xliii
4.11	Optical model radii with $U_{\text{sym}} = 4.4$ MeV and unequal geometries	xliv
5.1	DWBA calculations for L = 2 states	lv
5.2	DWBA calculations for L = 3 states	lvi
5.3	DWBA calculations for L = 4 states	lvii
5.4	DWVA calculations for L = 5 states	lviii
6.1	Comparison of ^{48}Ca and ^{50}Ti	lxi
6.2	Comparison of ^{48}Ca and ^{52}Cr	lxii
6.3	L = 3 states	lxv
6.4	L = 5 states	lxix
6.5	L = 4 states	lxxi
6.6	Comparison with other experiments	lxxix

6.7	Experimentally determined β^2	lxxx
I.1	Surface barrier geometry	xc
I.2	Detector mount	xciii
I.3	Slit scattering	xciv
I.4	^{137}Cs spectrum	xcvi
I.5	Alpha particle spectra	xxviii
I.6	Proton resolution at 40 MeV	xcix
I.7	Proton radiation damage	cii
I.8	Relative efficiency curve	cvi

1. INTRODUCTION

^{48}Ca is a doubly closed shell nucleus and is used as the core for a large number of nuclei in the $f_{7/2}$ region of the periodic table. Relatively little work has been done on ^{48}Ca because of the difficulty obtaining targets.* Inelastic alpha scattering performed at 42 MeV (Pe 65) and 31.5 MeV (Li 67) has identified the spins and parities of the strongly excited states, but the resolution of ~ 100 keV is not able to resolve many of the weak or high lying states. The $^{46}\text{Ca}(t,p)^{48}\text{Ca}$ reaction has been used to study the level structure of ^{48}Ca (Bj 67) and detects a large number of levels, but the experiment was only able to positively identify the 0^+ levels in ^{48}Ca . Inelastic proton scattering is able to identify angular momentum transfer reasonably well if the data are clean, and has the advantage of being a useful probe of the microscopic structure (Gl 66). Therefore the present experiment involving inelastic proton scattering was undertaken.

The ability of the (p,p') reaction to identify angular momentum transfer increases as the incident beam energy increases, also the direct reaction theory is expected to be more correct at higher energies where compound nuclear effects are small. The experiment was performed at four energies to check the consistency of the DWBA

* ^{48}Ca is a stable nucleus, but constitutes only 0.18% of the natural abundance of Ca.

method of analysis and the collective model calculations.

The experiment was performed with Ge(Li) counters because these detectors are able to give 30 keV resolution at 40 MeV, and they have the dynamic range needed to obtain the data in a reasonable period of time. A magnet spectrograph can yield better resolution, but at the time was not available. Stacks of Si(Li) counters, while able to detect 40 MeV protons, cannot do so with 30 keV resolution and clean valleys.

The experiment was performed with the goniometer of Ken Thompson (Th 69), which was designed specifically for use with Ge(Li) detectors. The detectors were fabricated in this laboratory. A discussion of the fabrication techniques is presented in Appendix I.

2. EXPERIMENTAL PROCEDURE

2.1 Modifications to the Goniometer

In order to obtain the data for this experiment in a "reasonable" period of time it was decided that a detection system that would allow simultaneous data taking at two angles was needed. Other requirements were that small angle data into 15° be taken, and that the only windows the scattered protons traverse be the 1/4 mil aluminized mylar windows on the detector cryostats. Therefore it was necessary to design a new 16" target chamber with a sliding seal for use with the goniometer (Th 69).

The modular design of the goniometer makes it particularly convenient for modification to particular experimental requirements. The details of the 16" target chamber are shown on MSUCL drawing HA-110-901-H. The basic design calls for input and exit ports compatible with the taped beam pipe and slip-fit O-ring seals used previously. The data taking window extends from 10° to 110° . There are two viewing ports opposite the data taking window that extend from 20° to 70° and from 110° to 160° . There is also a fixed Leybold fitting at 90° on this side of the chamber. On the data taking side of the chamber, there are two BNC feed throughs at 145° and 155° , and another Leybold fitting at 135° .

This particular design allows data to be taken from about 12° to 110° . If one wants to take data at scattering angles larger than 110°

the chamber may be rotated 180° and data taken from 70° to 170°. The monitor counter may be set on the secondary arm at any angle to view the beam through the monitor ports or at either of the fixed Leybold fittings.

The sliding seal is composed of a 1/8" O-ring inset in the chamber and a sliding steel strap made of 9 mil shimstock. Pressure sensitive teflon tape was applied to the chamber and the clamping ring to provide a smooth non-stick surface for the steel strap. In practice it was necessary to glue the O-ring into the groove in the chamber to prevent movement of the O-ring when the steel strap was moved. In addition the strap and O-ring were well lubricated with Dow Corning silicone high vacuum grease. No particular problems were encountered with the sliding seal in use as long as it was kept clean and lubricated.

The vacuum feed throughs to the detector cryostat caps were short sections of 3/4" copper tubing. The tubing was soldered into a brass block which was in turn soldered to the steel strap. The cryostat caps were coupled to the copper tubing using a simple O-ring slip fitting.

To provide the counter torque needed when the sliding seal is in motion, the target chamber was rigidly attached to a quadrupole support stand with a 1" X 5" aluminum arm. This same quadrupole support stand, which was bolted to the floor, was used to support the vacuum diffusion pump for the goniometer.

2.2 Target Storage System

The target used in this experiment was relatively expensive and

it would oxidize completely if exposed to the atmosphere for a few hours. Therefore, it was necessary to design and build a vacuum storage system for the target. The goniometer was initially designed with a target transfer lock which could be used to transfer a target into the target chamber without breaking vacuum (Th 69), therefore the target storage system was designed to be compatible with the transfer unit of the goniometer.

A modular design consisting of three basic units was used. A cryogenic pumping system with three ports, a transfer valve, and a storage chamber are the three basic units. The details for the target storage system are shown on MSUCL drawings HA-114-100-F to HA-114-106-F.

The cryogenic pumping system is based on a Linde LD-10 cryosorption pump attached to three NRC 1253-1 1/8" valves which are coupled to the standard 4" Marmon flanges. A cryosorption pump was used because a system was needed which was independent of probable university-wide power failures. While it is true that the pump must always be kept at liquid nitrogen temperature, it was not felt that this was a particular disadvantage, since the detectors also had to be stored at liquid nitrogen temperature and could be kept at the same dewar.

The second unit in the storage system is the storage-transfer valve. This is a vacuum valve which has 4" Marmon flanges on both sides, can hold a vacuum on either side, and is wide enough to allow passage of a 1 1/4" target frame in the open position.

The third unit is the storage chamber itself which is merely an aluminum chamber with a lucite window and a target holder.

To make a target transfer from the storage system to the goniometer

the portable storage system is moved out to the experimental area near the goniometer. The storage valve is closed and the storage chamber and valve removed from the cryosorption pump. The transfer unit (Th 69) is attached to the storage valve and then evacuated. The valve is opened and the target moved into the transfer unit. The valve is closed and the storage chamber is removed from the valve. The transfer unit with the target is now attached to the goniometer. When the goniometer is evacuated, the transfer valve is opened and the target is transferred to the target ladder of the goniometer. The complete transfer in vacuum requires about 45 minutes.

2.3 Cyclotron and Beam Transport

The Michigan State University sector-focused cyclotron (B1 66) was used to produce the proton beams used in this experiment. The machine is a variable energy, isochronous cyclotron utilizing an electrostatic deflector and magnetic channel for single turn extraction. The experiment was performed with an internal beam of 1 to 5 microamps. The extraction efficiency varied from 70% to 100%. The beam current on target was varied from 3 to 90 nanoamps depending on the scattering angle.

The extracted beam is focused and energy analysed by the beam transport system shown in Figure 2.1. The two horizontal bending magnets, M1 and M2, are used to center the beam on the object slit, S1, and to align the beam parallel to the beam pipe axis. The quadrupole doublets, Q1 and Q2, are used to focus the beam on slit S1. The divergence of the beam is defined by slits S1 and S2 which are separated

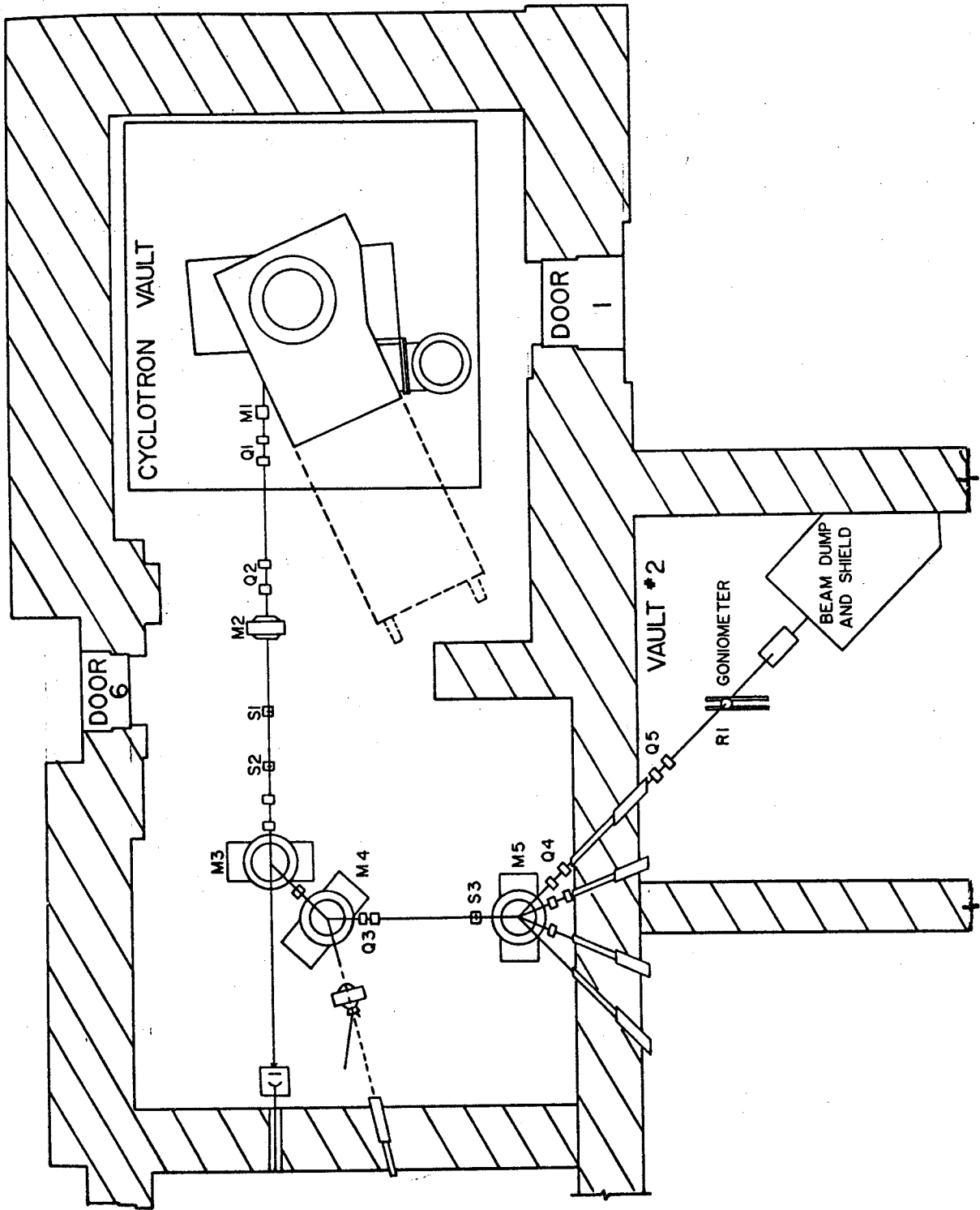


Figure 2.1 Cyclotron and beam layout.

by 48 inches. M3 and M4 are two 45° bending magnets which are the primary elements of the analysis system. The quadrupole doublet Q3 focuses the beam on slit S3. M5 is another 45° bending magnet which deflects the beam into the goniometer. The quadrupole doublets Q4 and Q5 focus the beam onto the target. More complete descriptions of the properties of the energy analysis system have been published elsewhere (Ma 67) (Sn 67). During this experiment the slits S1 and S3 were set at 15 mils for energy resolution of 10 keV. S2 was set at 100 mils to yield a beam divergence of ± 2 mrad.

For the final beam preparation a scintillator with a 1/8 inch hole in the center was inserted in the target ladder of the goniometer. The beam spot was viewed with a television camera to check for proper focus and centering. In addition a tantalum ring, R1, with a 1/2 inch hole was located 16 inches in front of the target on the beam axis. The beam current on this ring was monitored throughout the experiment. The criteria used to insure proper alignment of the beam were: a well focused and centered beam on the scintillator, minimum current on the ring, maximum current in the Faraday cup, and minimum neutron background in the experimental room.

During the experiment the beam spot on target was approximately 1/16 inch wide and 3/8 inches high. The current on the ring was always less than 1% of the beam dumped in the Faraday cup and was usually 0.1% or less. The current on the ring was probably due to slit scattering from S3. The neutron background in the experimental area provided a very sensitive test of the alignment of the beam into

the goniometer. If the beam scraped the beam pipe, the input snout, or the exit snout it would increase the neutron background by 2 or 3 orders of magnitude.

The Faraday cup used in this experiment is actually only a shielded beam dump and as such was not intended to measure absolute charge accurately. A 12 foot section of beam pipe, insulated from the goniometer by a Delrin spacer, with a 1/2 inch thick aluminum cap was used. It was surrounded by concrete and paraffin shielding described elsewhere (Th 69a) to reduce the neutron background seen by the detectors.

The Faraday cup was in contact with the paraffin and concrete shielding blocks and was probably subject to some leakage current to ground. The Faraday cup was connected to an Ortec model 439 current digitizer used with an Ortec model 430 scaler to integrate the charge. The current digitizer outputs a logic pulse for every 10^{-10} Coulomb of integrated charge. This logic pulse is then fed into the scaler to record the total integrated charge. This arrangement provided relative numbers for the total incident charge for each run; these numbers were used as a check on the monitor counter which was used for the actual normalization.

2.4 Detectors

The detectors used in this experiment were lithium drifted germanium counters of the surface barrier geometry designed specifically for this experiment. (See Appendix I) The two detectors were

separated by 14.6° . The small angle counter was 13.25 inches from the target and had a final 30 mil Ta collimator that was 6.6 mm high and 2.2 mm wide. The large angle counter was 11.25 inches from the target and had a final 30 mil Ta collimator that was 6.2 mm high and 2.2 mm wide. The two detectors were operated at 1500 V and 1200 V bias respectively with leakage currents of less than 0.1 na.

The monitor counter used in this experiment was also of the Ge (Li) type, but since optimum resolution was not required, it was used in the side entry geometry. The detector was mounted in a Harshaw cryostat of the "sausage" type (Model 15). The monitor counter was mounted at a fixed angle on the secondary arm of the goniometer. The protons scattered into the monitor counter traversed an air space of about 1/2 inch between the 1/2 mil Kapton window on the target chamber of the goniometer and the 1/4 mil aluminized mylar window on the cryostat.

2.5 Electronics

The electronic equipment used in this experiment is shown in Figure 2.2. At the time the experiment was performed, it was necessary to use rather unconventional arrangement of the electronics to obtain acceptable resolution. It was our experience that with commercially available electronics, after amplification to the required 5 to 10 volt output signal, the rms noise level would be 3 to 4 mV, thus yielding a precision of 0.04% to 0.06% in the voltage measurement. At 40 MeV this corresponds to a contribution of 16 to 24 keV to the overall resolution. This was not acceptable.

It was found that by using a modified Ortec 109A preamplifier and the second stage of the Tennelec TC200 amplifier, the total electronic noise as measured with a Canberra stabilized pulser (Model 1501) was less than 6 keV at 40 MeV. The outputs of the amplifiers were fed into two Northern Scientific NS 629 analog-to-digital converters. The ADCs were interfaced to a Sigma 7 computer which was used to store the data. The ADCs were set to provide 8192 channel conversion gain. Only the upper 4096 channels of information were stored by using the 4096 channel digital offset. Using this configuration spectra were obtained with about 5 keV per channel.

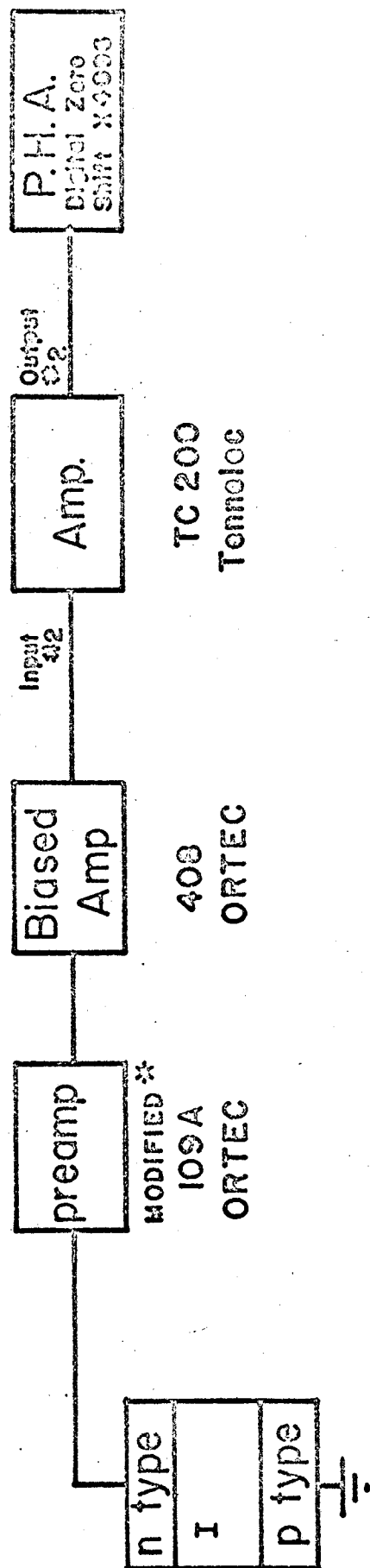
Conventional electronics were used with the monitor counter: Ortec 109A preamplifier, Ortec 410 linear amplifier, Ortec biased amplifier and into a Nuclear Data 160 multichannel analyser.

To make the dead time corrections two Ortec 420 single channel analysers were used. A window was set on the elastic peak from the monitor counter; the output of the single channel analyser was used to feed an Ortec 430 scaler and the channel zero of each NS 629 ADC. The Ortec 416 gate and delay generator was used to provide proper pulse shaping for the ADCs. The dead time correction was made by comparing the number of counts in the scaler with the number of counts in channel zero. A similar arrangement was used to make the dead time corrections for the monitor counter. The dead times throughout the experiment were always less than 5%.

2.6 Data Acquisition

The data were acquired during two three day runs. Data for

Electronics for Ge(Li) detector



Typical precision of electronics: 0.015% at 40 MeV

* Modified by Joel B. Ayres, ORTEC

Figure 2.2 Ge(Li) electronics.

each energy were taken at 20 angles in 5° steps from about 13° to 100°. The data at 28° and 73° were taken twice, once with each put in position for aligning the beam at the next energy. The counters were removed during the alignment procedure to prevent radiation damage from the neutron background.

The resolution obtained during this experiment was between 25 and 30 keV (FWHM). The contributions to this energy resolution are listed in Table 2.1. Notice that the straggling contributions from the windows add directly rather than an quadrature, and they are the largest contribution to the energy resolution.

Table 2.1 Contributions to the energy resolution

Source	$\Delta E(\text{keV})$	$\Delta E^2(\text{keV}^2)$
Electronics	6.0	36
Ion pair statistics	6.2	39
Nuclear collisions	0.7	
Straggling		
Target 5	18.3	337
Package window 5.3		
Detector window 8		
Beam	10	100
Kinematics	10	100
Total	<u>24.5</u>	<u>602</u>

Representative spectra at each energy are shown in Figures 2.2 - 2.5.

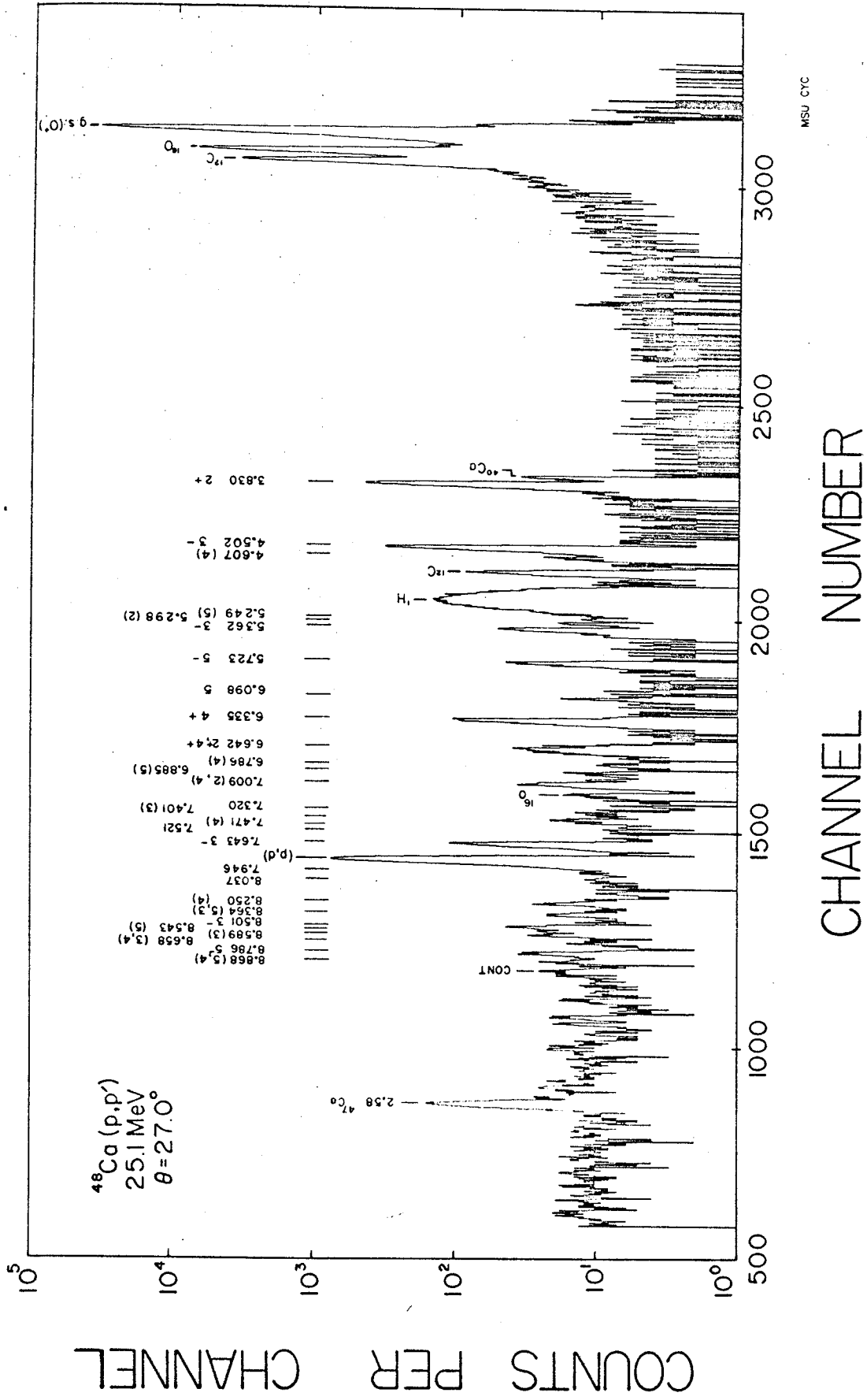


Figure 2.3 Typical 25 Mev spectrum.

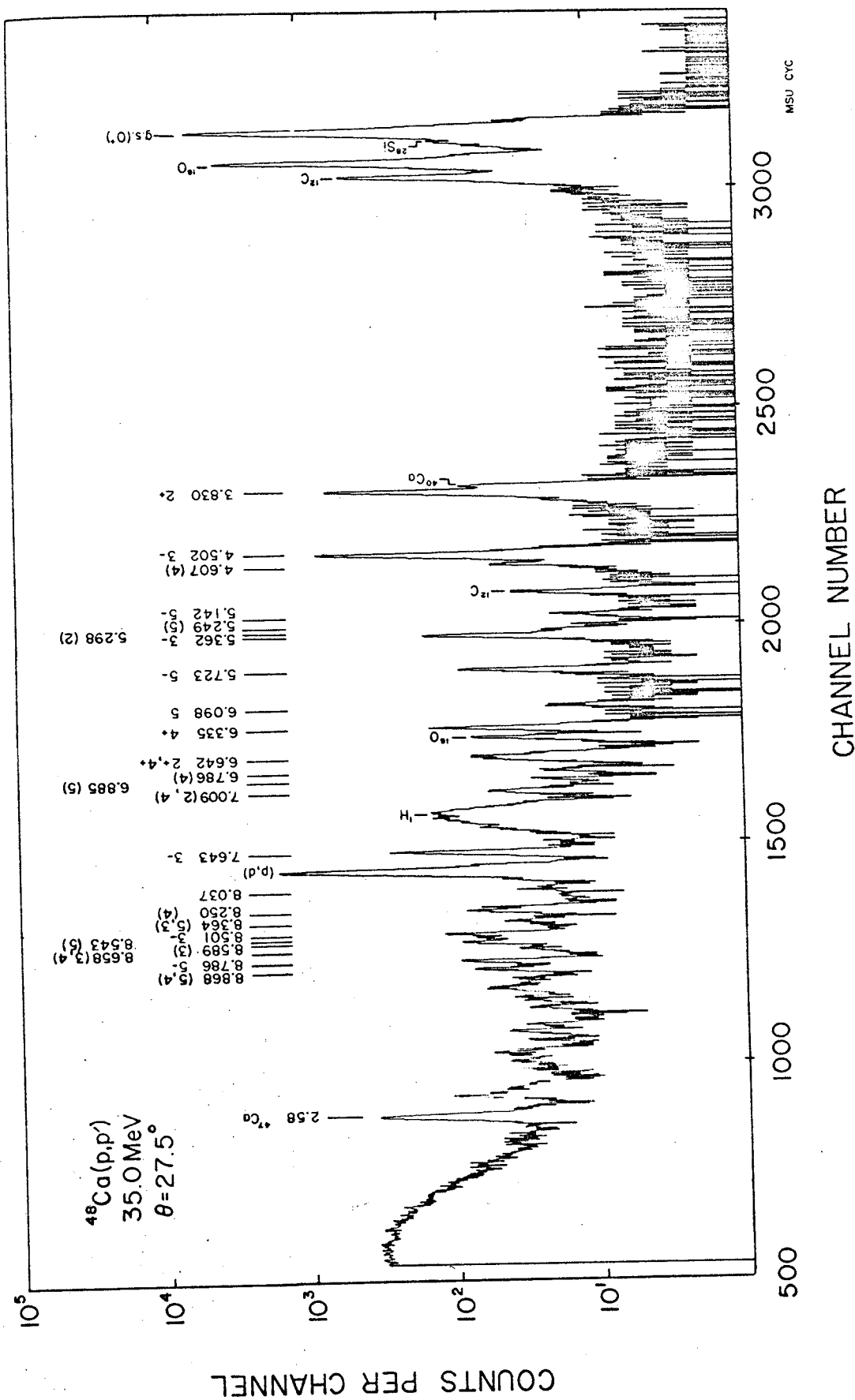


Figure 2.5 Typical 35 Mev spectrum.

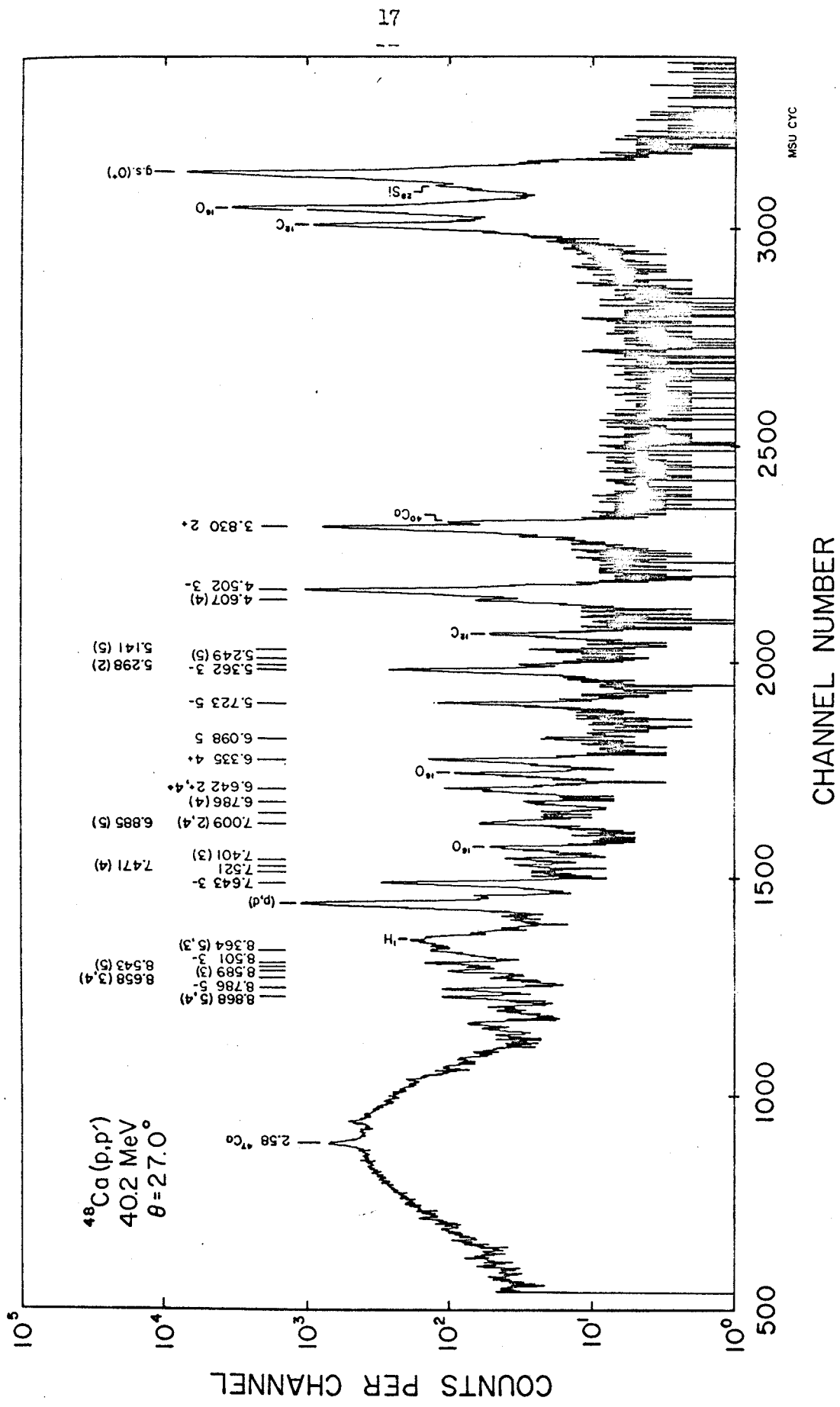


Figure 2.6 Typical 40 Mev spectrum.

3. DATA ANALYSIS

In this experiment the relative cross sections were measured using a monitor counter for normalization. The absolute cross sections were obtained by normalizing the ^{40}Ca elastic scattering, observed at large angles, to previous work and using the ratio of isotopic abundances in the target (c.f. Sec. 3.2).

The use of a monitor counter at a fixed angle to provide the relative normalization for each run eliminated the need to know the exact areal density of the target, solid angles of the detectors, target angle, and total incident charge.

The relative normalization between the two detectors used in this experiment was determined by taking data at a number of overlap angles. Dead time corrections were made for both detector ADC's as well as the monitor counter ADC.

3.1 Angle Calibration

The program, PEAKSTRIP, written by R. A. Paddock, was used to obtain the centroid, net counts, and statistical error in the counts for each peak in the spectrum. The input consisted of the two channel numbers, defining the edges of each peak, and the backgrounds at these boundary channels. A linear background is assumed under the peak. If there were more than 30 counts in the peak, the centroid was determined using the top two-thirds of the peak; otherwise the total peak was used.

The fractional standard error for the counts in each peak was determined by the formula

$$\Delta N = \frac{(N + 2B)^{1/2}}{N}$$

where

N is the total number of counts and

B is the total background count.

To determine the scattering angle for each spectrum the computer program, ANGAL, was written. The program input consists of the centroids of three uncontaminated peaks, one of which is moving kinematically faster than the other two. The two slowly moving peaks are used for energy calibration, the third peak is used to determine the angle. An initial guess is made for the angle, and then, through an iterative procedure, the actual scattering angle is determined. The process usually converges within four iterations. Relativistic kinematics, calculated by the program KINE, written by P. J. Plauser, are used throughout. Typically elastic scattering from H or ^{12}C was used for the fast moving peak, and the ground state and known excited states of ^{48}Ca (Ma 66) (Bj 67) were used for the kinematically slow moving peaks. The angle calibration determined by the above procedure is believed accurate to $\pm 0.1^\circ$; the major limitations are the accuracy with which the centroid can be determined, the uncertainty in the energy calibration curve, and the uncertainty of the incident beam energy.

3.2 Normalization

The relative normalization for each run was obtained by

normalizing to the total counts in the elastic peak observed by the monitor counter. In each monitor spectrum the edges of the elastic peak were chosen at a constant fraction of the total peak height. The ratio of monitor counts to the integrated current for each run was calculated and found to be constant to within 5%. It is believed that the monitor counter yields the better relative normalization since the current digitizer and Faraday cup were subject to some leakage current.

Since data were taken simultaneously at two angles during the experiment it was necessary to determine the relative normalization between counters. This normalization is determined by the difference in solid angle subtended by the two counters and any difference in the detection efficiency of the two counters. The relative normalization between counters for this experiment was determined by taking data over the same angular range with each counter and then normalizing one angular distribution to the other. This was done at each energy and found to be constant within 2%. If a large error were made in the relative normalization between counters, the error would show up as systematic discontinuities in the angular distributions of all states at the overlap angles where one counter started taking data and the other stopped. No such discontinuities in the angular distributions were observed.

At scattering angles greater than 65° this experiment was able to completely resolve the elastic scattering from ^{40}Ca and ^{48}Ca . Table 3.1 lists the composition of the target used in this experiment.

Table 3.1 Isotopic analysis of the target.*

Isotope	Atomic %	Precision
40	3.58	± 0.05
42	0.05	± 0.01
43	0.01	
44	0.11	± 0.02
46	< 0.01	
48	96.25	± 0.05

* Determined by the Stable Isotopes Division of the Oak Ridge National Laboratory where the target was made.

Table 3.2 Contributions to the uncertainty in absolute normalization.

Source	%
Target composition	2
Normalization of ^{40}Ca	5
Statistics: ^{40}Ca peak	7
Monitor peak	3
Total	$\sim 10\%$

It can be seen that ^{40}Ca is the major contaminant and the relative amount is determined to within 5%. Accurate elastic scattering data for ^{40}Ca already exists (Fr 67); therefore it was decided to normalize the present ^{48}Ca data using the ratio of isotopic abundances in the target. As can be seen from Table 3.2, the absolute cross sections determined in this manner are accurate to $\pm 10\%$. The principal contributions to the uncertainty are the statistics of the ^{40}Ca elastic peak and the absolute normalization of the ^{40}Ca elastic scattering.

3.3 Excitation Energies

To determine the excitation energies of the various states observed, the program FOILTARCAL, written by R. A. Paddock, was used. The input was the output of PEAKSTRIP plus information concerning target composition, target orientation, the reaction involved, the detector angle, and a set of standard reference peaks. The program uses the reference peaks to determine a calibration curve of given order, which is then used to find the excitation energies of the unknown peaks. The program accounts for target thickness and uses relativistic kinematics throughout.

The reference peaks used for calibration purposes were the ground states of ^{48}Ca , ^{16}O , ^{12}C , the 4.44 MeV state of ^{12}C , the excited states of ^{48}Ca listed in Table 3.3, and the (p,d) ground state. Only reference peaks that were free of contaminants were used.

In order to use the deuteron peak as a calibration point in

the proton spectrum it was necessary to make a correction for the window in front of the detector. Since the deuteron loses more energy than a proton of the same energy in traversing the 1/4 mil aluminized mylar window, it was necessary to calculate the difference in energy loss between a proton and deuteron of the same energy and add this correction factor to the excitation energy of the deuteron. This correction factor varied from 20 to 60 kilovolts depending on the energy and angle of the scattered deuteron.

Both linear and quadratic energy calibration curves were tried. It was found that both linear and quadratic calibration curves yielded excitation energies for known states that agreed with those of Marinov and Erskine (Ma 66) to within the calculated uncertainties. As might be expected the quadratic curve yielded a better absolute fit to the known excited states up to 7 MeV in excitation energy.

As a check on the calibration curve above 7 MeV, the deuteron peak corresponding to the 2.580 - 2.600 doublet in ^{47}Ca was used. Again the necessary corrections to make the deuteron look like an equivalent energy proton were made. The linear calibration curve predicted the position of the deuteron doublet to within 7 keV with an uncertainty of ± 11 keV. The quadratic calibration curve predicted an excitation energy for the doublet that was approximately 50 keV high.

Without strong evidence to indicate that a quadratic or higher order calibration curve was needed, it was decided that the linear energy calibration curve would be used. These results indicate that

Table 3.3 Excitation Energies of ^{48}Ca .

E^* (MeV) Present Data	E^* (MeV) Ma 66 (p,p')	E^* (MeV) La 66 (p,p')	E^* (MeV) Bj 66 (p,t)
3.830±0.005	3.833 [†]	3.818	3.827 [†]
	4.284	4.272	4.281
4.502±0.004	4.506 [†]	4.498	4.496 [†]
4.607±0.006	4.613	4.604	
5.142±0.004	5.146	5.13	
5.249±0.008		5.266	
5.298±0.007			
5.362±0.005	5.368 [†]	5.37	
			5.459
5.723±0.004	5.728	5.724	
6.093±0.008	6.106	6.096	
6.335±0.005	6.338 [†]	6.34	6.329 [†]
6.642±0.009		6.61	6.645
6.786±0.008		6.79	6.793
6.885±0.008			
7.009±0.008			
7.320±0.025			
7.401±0.025			
7.471±0.025			
7.521±0.025			
7.643±0.006			7.650
7.786±0.007			
7.940±0.006		7.97	
8.037±0.009			8.018
8.250±0.008			8.237
8.364±0.010			8.268
			8.473
8.501±0.008			8.513
8.543±0.008			8.538
8.589±0.007			8.604
8.658±0.010			
			8.697
8.786±0.008			8.782
8.868±0.008			

[†]Points used to determine the energy calibration curve.

the detectors and electronics used in this experiment yielded a data taking system which was linear to within 0.1% over a 10 MeV range of excitation energy.

3.4 Cross Sections

The program RELTOMOM, written by R. A. Paddock, was used to convert the PEAKSTRIP output and the monitor counts into the center-of-mass cross section for each peak. It was at this point that spurious data points were reanalyzed. Whenever possible, corrections were made for contaminated peaks.

In particular ^{12}C , ^{16}O , and ^{40}Ca were subtracted from the forward angle elastic scattering. To make these corrections the cross sections of the elastic scattering from ^{12}C and ^{16}O were used, where kinematically separated, to determine the relative amounts of carbon and oxygen on the target at each energy. Using the known ^{12}C and ^{16}O cross sections (Ca 67), the background subtraction could be made at smaller angles. The total amount of ^{12}C and ^{16}O on the target was approximately constant throughout the experiment. The same technique was used to subtract the excited states of ^{40}Ca from the ^{48}Ca excited states when they were not kinematically separated.

4. OPTICAL MODEL STUDIES

In order to perform the distorted wave Born approximation calculations, it is necessary to obtain the optical potential which describes the elastic scattering at each energy, because it is used to define part of the wave function in the entrance and exit channels. The optical potential is also of interest in itself because the parameterization used to describe the optical potential defines a radius which is usually associated with the matter distribution. Since good proton elastic scattering data exist for ^{40}Ca (Ku 70) (Fr 67) the study of the difference between elastic scattering from ^{40}Ca and ^{48}Ca and its relation to the optical model was undertaken.

4.1 Optical Model for DWBA Calculations

A commonly used optical potential, which has been found adequate to describe cross section and polarization data throughout the periodic table (Fr 67), is of the form

$$V(r) = V_c(r) - V_0 f(x_0) - i(W_0 - 4W_D \frac{d}{dx_I})f(x_I) + (h/m_p c)^2 V_S \frac{1}{r} \frac{d}{dr} f(x_S) \frac{1}{a_S}$$

V_c is the Coulomb potential for a uniformly charged sphere of radius $1.25 A^{1/3}$. The geometry is of the Woods-Saxon form, that is

$$f(x_i) = [1 + \exp(x_i)]^{-1} \text{ where}$$

$$x_i = (r - r_i A^{1/3})/a_i.$$

Fricke *et. al.* found a set of average optical potential parameters which fit a large number of targets. These parameters are listed in Table 4.1.

Table 4.1 Fricke's average optical parameters.

$r_o = 1.16F$	$a_o = 0.75F$
$r_I = 1.37F$	$a_I = 0.63F$
$r_s = 1.06F$	$a_s = 0.738F$
$V_s = 6.04 \text{ MeV}$	

It was found that by using these average geometry parameters a reasonable fit to the elastic scattering data could be found by searching on the potential well depths V_o , W_o , and W_D . The optical model search code, GIBELUMP, was used to minimize χ^2 by varying the potential well depths. The quantity χ^2 is a measure of the goodness of fit of the theory to the data.

$$\chi^2 = \frac{1}{N} \sum_{i=1}^N [(\sigma_{Th}(\theta_i) - \sigma_{Ex}(\theta_i)) / \Delta\sigma_{Ex}(\theta_i)]^2$$

where N is the number of points, $\sigma_{Ex}(\theta_i)$ and $\sigma_{Th}(\theta_i)$ are the experimental and theoretical cross sections at the angle θ_i , and $\Delta\sigma_{Ex}(\theta_i)$ is the experimental error associated with the i^{th} data point. The final parameters used at each energy are listed in Table 4.2.

Table 4.2 Potential well depths using Fricke geometry.

Energy (MeV)	V_o (MeV)	W_o (MeV)	W_D (MeV)	χ^2/N
25.11	50.98	0.60	6.04	11
29.83	49.93	3.96	3.61	11
35.00	48.80	5.24	2.34	7
40.21	47.67	5.24	2.35	4

The fits provided by these parameters to the data are shown in Figure 4.1.

In extracting a deformation parameter δ for the inelastic scattering (see Section 5.) there is a possible ambiguity due to the fact that the real and imaginary geometries are not equal. Therefore, a set of optical parameters were found with the additional constraint that the real and imaginary geometries be equal. In this analysis $r_o = r_I = 1.20F$ and $a_o = a_I = 0.68F$. The optical strength parameters are listed in Table 4.3.

Table 4.3 Potential well depths with equal real and imaginary geometries.

Energy (MeV)	V_o (MeV)	W_o (MeV)	W_D (MeV)	χ^2/N
25.11	51.72	0.36	6.95	13
29.83	45.93	0.15	6.57	6.4
35.00	46.50	3.49	4.62	3.6
40.21	46.58	4.13	4.57	2.0

The fits to the data are shown in Figure 4.2.

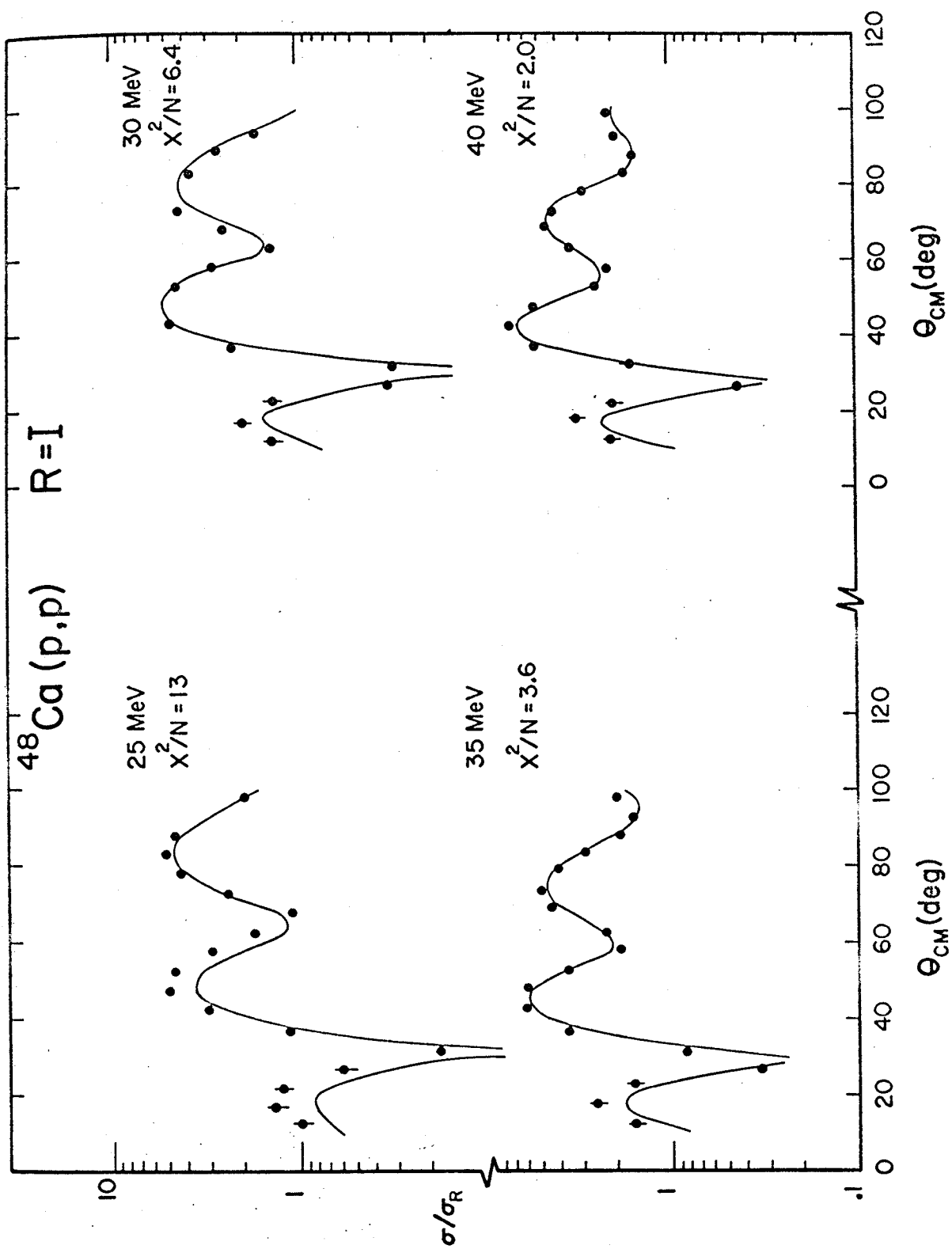


Figure 4.1 Optical Model fit with $R=I$ geometry.

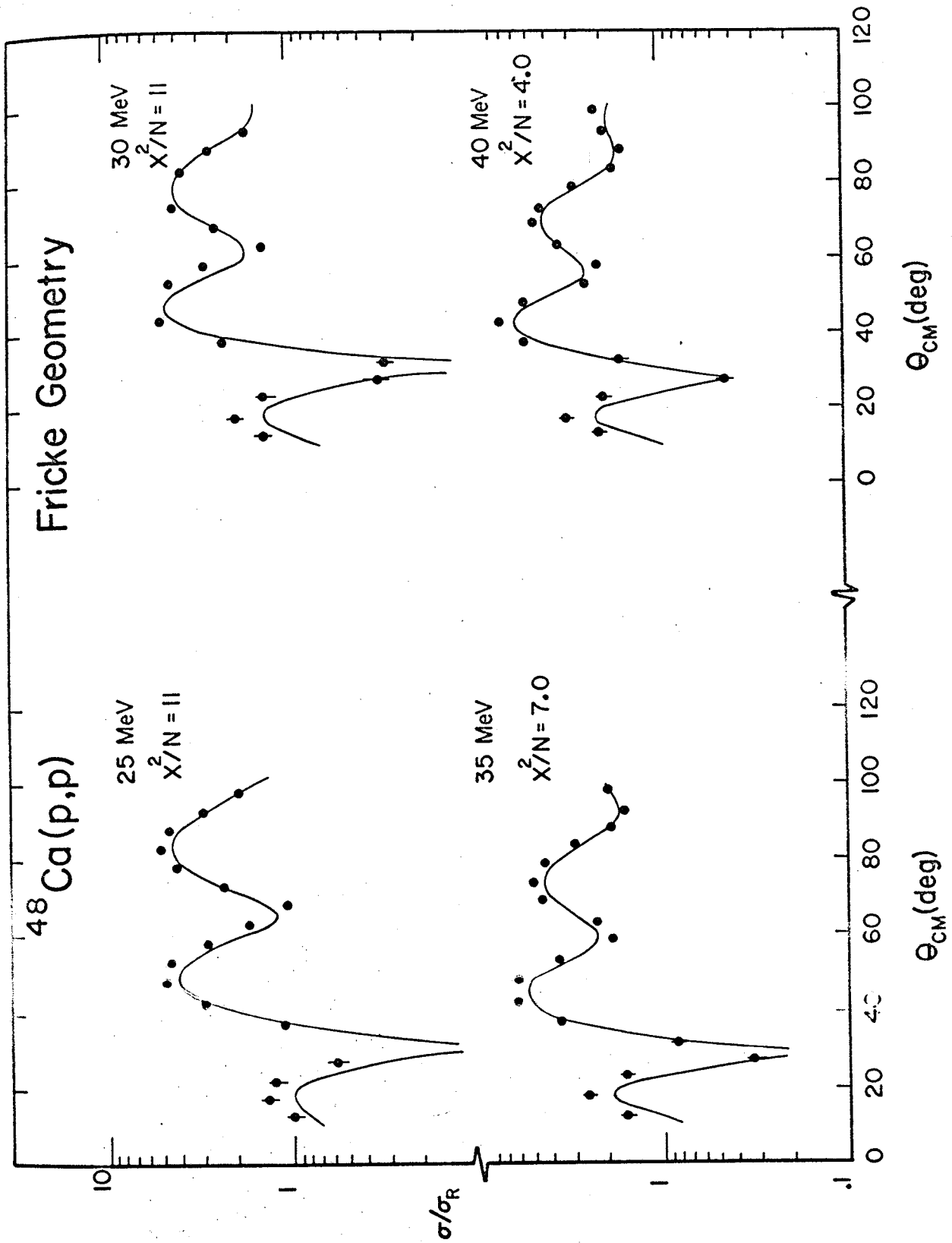


Figure 4.2 Optical model fit with Fricke geometry.

4.2 Optical Model Difference Between ^{40}Ca and ^{48}Ca

Electromagnetic studies of the relative charge distributions of the calcium isotopes indicate that for ^{48}Ca relative to ^{40}Ca , the half density point of the charge distribution (R_{op}) increases by 0.15F and the surface diffusivity decreases by 12%. (Fr 68) Recent optical model analyses of 30 MeV elastic alpha scattering from these nuclei by Bernstein, et. al. indicate that $\Delta R_{op} = R_{op}(^{40}\text{Ca}) = 0.15F$ and the surface diffusivity is essentially unchanged (Ee 69). Fernandez and Blair have calculated a strong absorption radius for 42 MeV elastic alpha scattering and also find $\Delta R \approx 0.15F$ with the diffusivity being a constant. (Fe 70)

If one assumes that the matter distribution is related to the geometry of the optical potential used to fit the elastic scattering, then one may be able to determine differences in the matter distribution by looking at differences in the optical potential. We have therefore used the optical model to fit the ^{40}Ca data and fix the potential well depths at each energy. The ^{48}Ca data are then fit by using the potential strengths obtained from the ^{40}Ca analysis and performing a search which grids the parameters determining the geometry of the optical model. Such a grid search was performed so that the sensitivity of the fit to the radius and diffusivity would be determined.

The optical model with its large number of parameters presents a problem in itself since many of the parameters are known to be coupled. It was therefore decided to simplify the potential as much

as possible. The spin-orbit potential did not improve the fit to the data, particularly since polarization and large angle data were not being fit. Therefore, the spin orbit terms were eliminated entirely with no effect on the results presented here. One possible optical potential would have a Coulomb term and either a surface or a volume imaginary term along with the real volume term. In this potential the real and imaginary terms have the same geometry. As a first try, therefore, a potential of the following form was used:

$$U(r) = U_C(r) - [V_R - i4W_D] f(x)$$

$$f(x) = (1 + e^x)^{-1} \text{ where } x = \frac{(r - r_0 A^{1/3})}{a}$$

This is essentially the same potential used by Bernstein et. al. in their alpha particle analysis except that a surface absorption rather than volume absorption term is used. The procedure was to fix the geometry for the ^{40}Ca analysis ($r_0 = 1.25$ fm, and $a = 0.65$ fm) and search on V_R and W_D to obtain the best fit at each energy. Then a "geometric" analysis of the ^{48}Ca data was made by holding V_R and W_D the same for both isotopes and performing a grid search on r_0 and a .

An immediate objection to the procedure of holding V_R the same for both nuclei can be made since there is a symmetry term in the real central potential of the form $V_{\text{SYM}} \frac{(N-Z)}{A}$. (S1 63) This is particularly important if one is trying to describe differences in the elastic scattering by differences in the geometry because of the Vr^2 ambiguity in the optical model. (Pe 62) Therefore a grid search

was also performed for the ^{48}Ca data where $V_R(^{48}\text{Ca}) = V_R(^{40}\text{Ca}) + V_{\text{SYM}} \frac{(N-Z)}{A}$. The value of V_{SYM} used was 26.4 MeV (Fr 67) which added 4.4 MeV to the real well depth of ^{40}Ca . The results of a grid search on r_0 and a are most easily visualized using an iso- χ^2 plot as in Figure 4.3. It can be seen that the radius has a more well defined minimum in χ^2 space than the diffusivity and that the two parameters are slightly coupled. Plots at the other energies are shown in Figures 4.4, 4.5, and 4.6. Notice that the minimum in χ^2 for the 25 MeV data is not well defined as a function of diffusivity.

To investigate the sensitivity of the results to the form of the imaginary potential, the same calculations were performed using volume absorption only and a combination of volume and surface absorption. The quality of the fit at any given energy varied depending on the form of the imaginary potential. The higher energy data was fitted better with more volume absorption and the lower energy data was fitted better with more surface absorption. The geometry parameters yielding a best fit in each case were, however, approximately independent of the form of the imaginary potential at each energy.

Elastic proton scattering is often fit with an optical model having a different real and imaginary geometry. The sensitivity of the results to the requirement that the real and imaginary geometries be equal was investigated by using the geometry parameters of Fricke, et. al. (Fr 67) for the ^{40}Ca data. The results at each energy are listed in Table 4.4 and are in reasonable agreement with the results obtained by holding the real and imaginary geometries equal. The

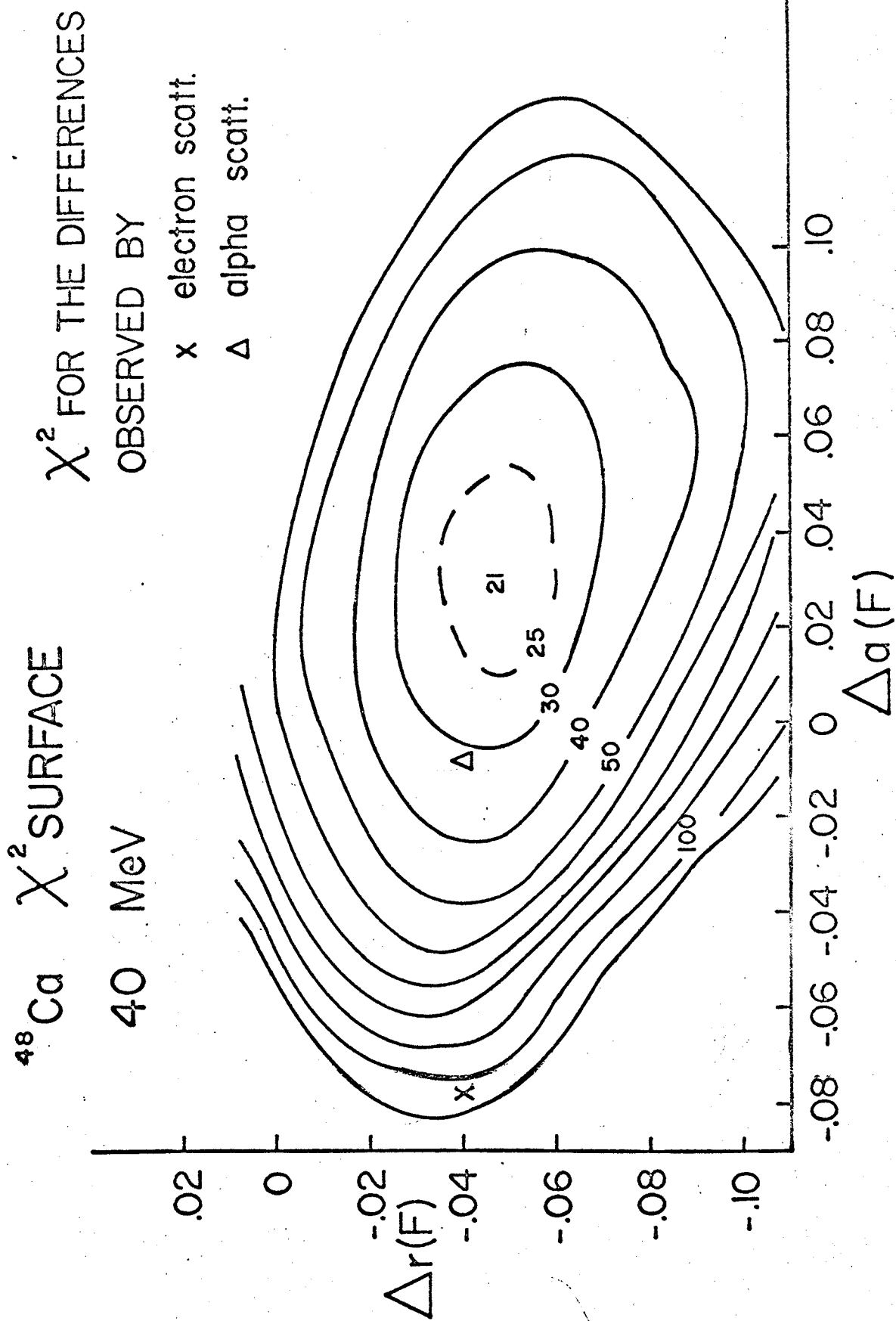


Figure 4.3 40 Mev χ^2 surface.

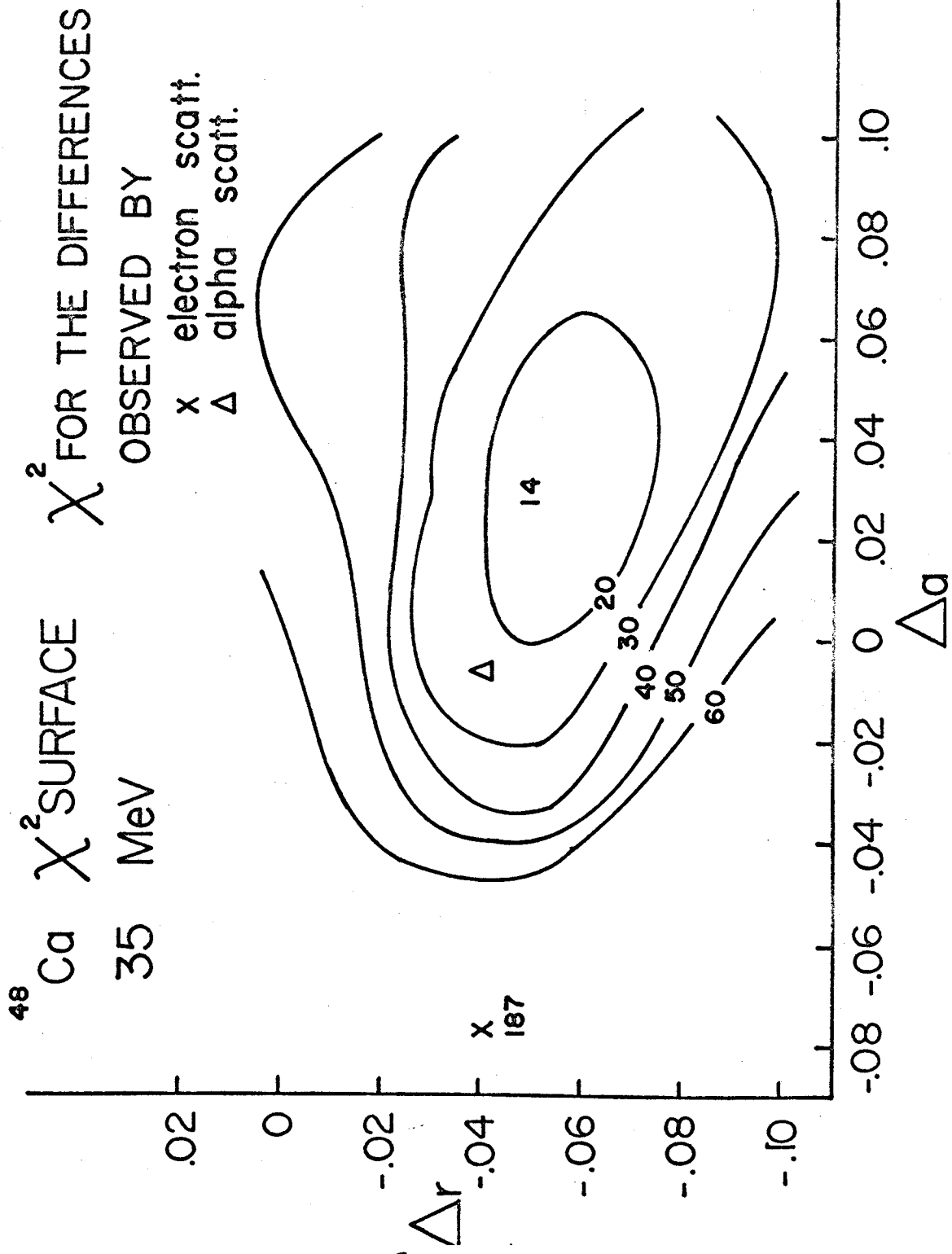


Figure 4.4 35 Mev χ^2 surface..

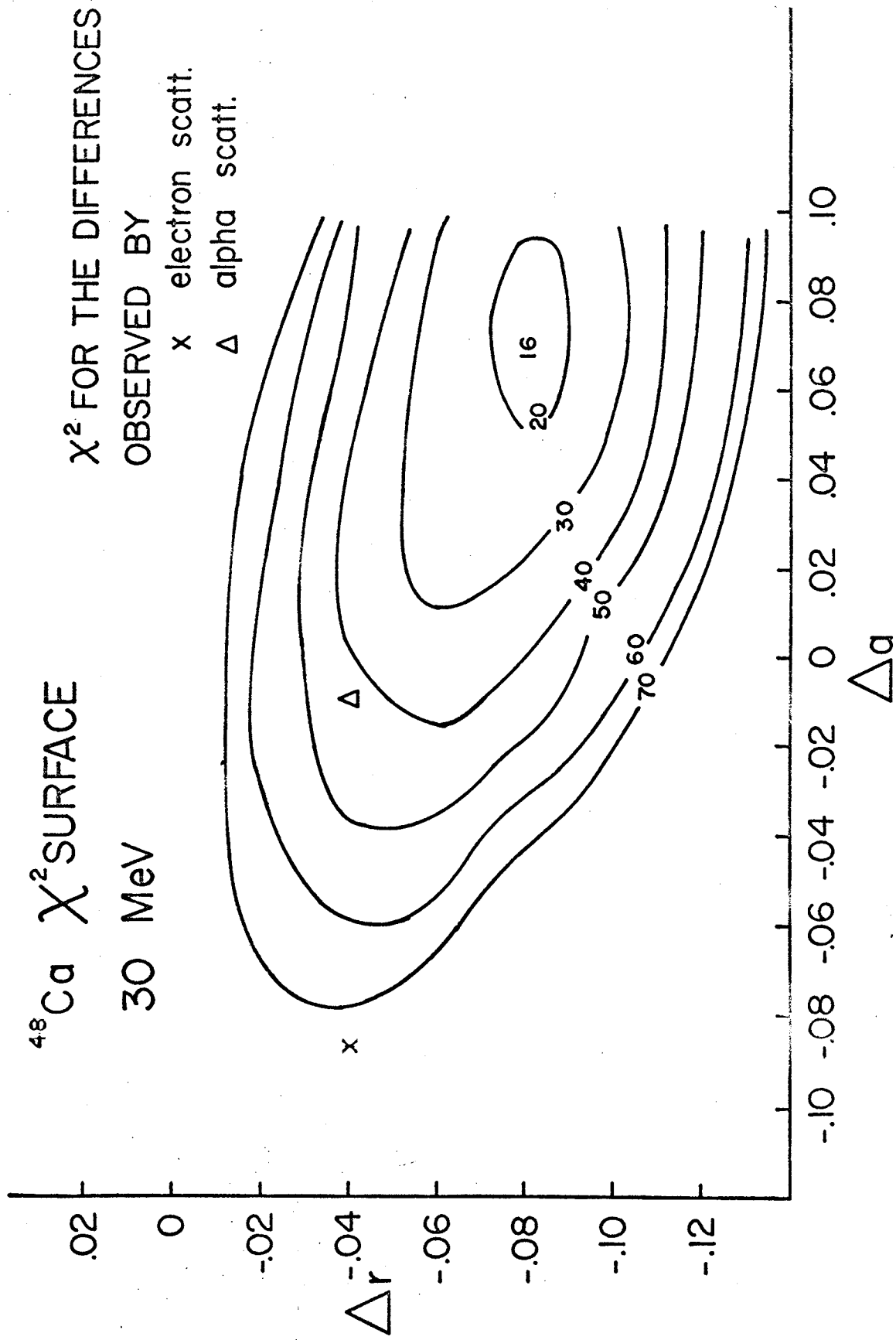


Figure 4.5 30 MeV χ^2 surface.

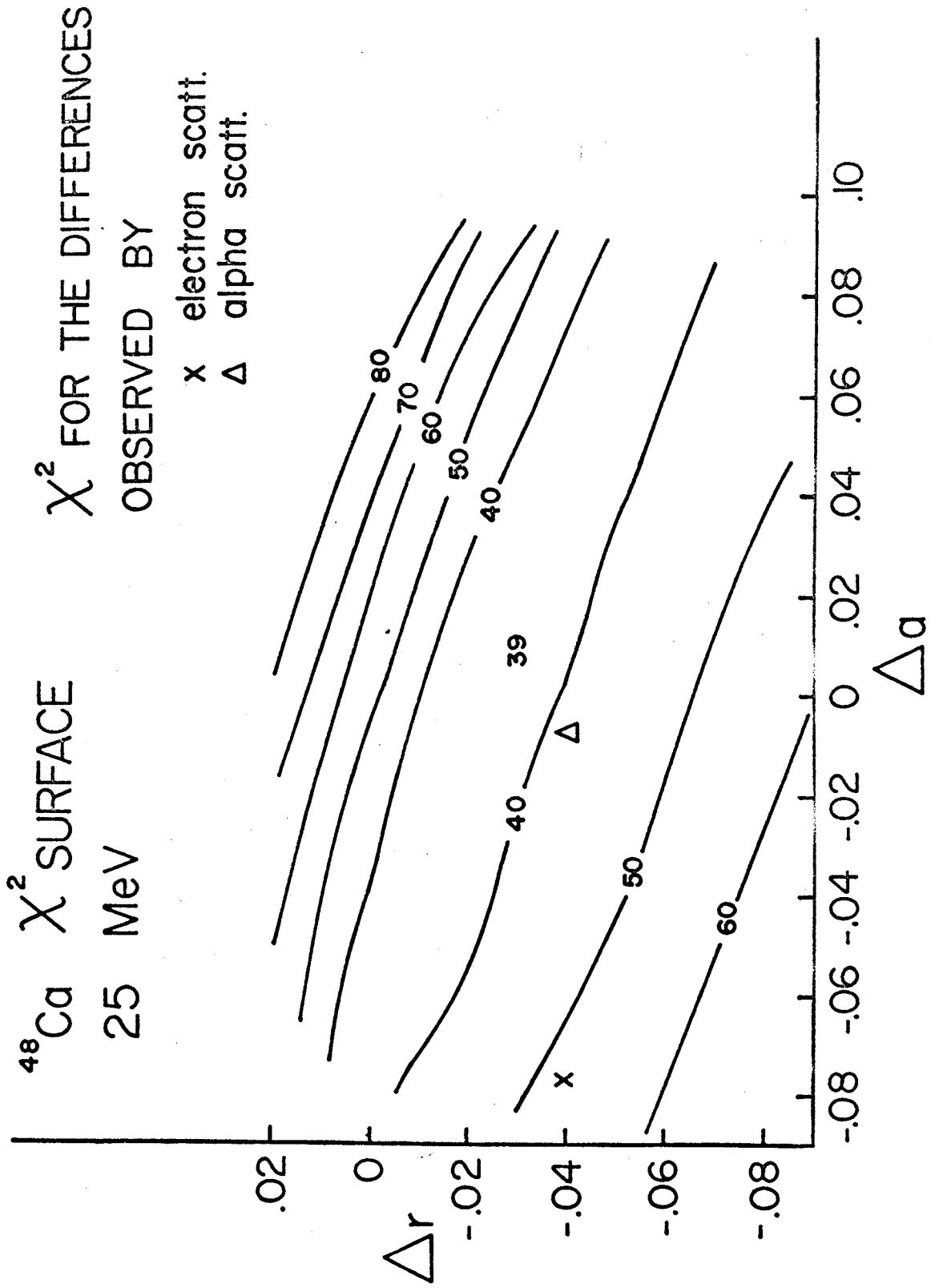


Figure 4.6 25 Mev χ^2 surface.

